Near infrared and hyperspectral studies of archaeological stratigraphy and statistical considerations

Johan Linderholm, Paul Geladi, Nathalie Gorretta, R. Bendoula, Alexia Gobrecht

Received: 16 January 2018 | Revised: 2 July 2018 | Accepted: 25 November 2018

DOI: 10.1002/gea.21731

RESEARCH ARTICLE

WILEY Geoarchaeology An International Journal

Near infrared and hyperspectral studies of archaeological stratigraphy and statistical considerations

Johan Linderholm[1] | Paul Geladi[2] | Nathalie Gorretta[3] | Ryad Bendoula[3] | Alexia Gobrecht[3]

[1]Department of Historical, Philosophical and Religious Studies, Umeå University, Umeå, Sweden

[2]Department of Forest Biomaterials and Technology, Swedish University of Agricultural Sciences, Umeå, Sweden

[3]UMR ITAP, IRSTEA, Centre de Montpellier, Montpellier, France

Correspondence
Johan Linderholm, Department of Historical, Umeå University, Philosophical and Religious Studies, SE 90187 Umeå, Sweden.
Email: johan.linderholm@umu.se

Funding information
Marcus & Amalia Wallenberg Foundation, Grant/Award Number: MAW 2012.0136; The Kempe Foundation, Grant/Award Number: SMK-1749

Scientific editing by Sarah Sherwood

Abstract

The paper proposes a methodology based on near-infrared (NIR) spectrometry for studying stratigraphy and depth profiles in archaeological excavations. The NIR spectra can be used to describe and complement the wet chemical analysis. Soil samples were collected from a 0.8 m deep stratigraphy of a Neolithic site that were analyzed by three different NIR instrumentations. Phosphate- and magnetic susceptibility and inductively-coupled plasma mass spectrometry measurements were also conducted as reference analysis.

Principal component analysis on the data from three different NIR instrumentations gave useful score plots that allowed grouping of the samples. The results from the lab spectrometer were most useful, although the hyperspectral NIR camera was the fastest method to obtain spectra of many samples from one image. The paper shows how the NIR spectral data can be used for multivariate analysis to get meaningful conclusions on archaeological soils and sediments, especially in terms of understanding site development/phases and soil formation.

KEYWORDS
archaeological stratigraphy, chemometrics, hyperspectral Imaging, near infrared spectroscopy, soil formation

1 | INTRODUCTION

In archaeology, stratigraphy and soil depth profiles are important because they can reveal human settlement activities as a function of time, soil formation, processes of sedimentation and deposition. Important indicators of human settlement and human activities are redistribution and reworking of soils and sediments (Goldberg & Macphail, 2006). Also, accumulation of soil-phosphate (emanating from general waste, dung, and bones) (Holliday & Gartner, 2007) and of carbon compounds (accumulated organic matter and from the use of fire) into the soil system are general features. Soils and sediments from archaeological sites often differ significantly in this respect from the general background as they become recipients of waste and general amelioration, resulting in an excess of 10–100 times of phosphate content and other nutrients compared with the background. The organic matter that accumulates oxidizes and decomposes over time but is incorporated in the humic matter and retains some of its chemical properties or "signatures". An improved understanding of this process and the nature of these soils will improve the understanding of the cultural processes forming them but that requires some form of analysis results as a function of depth.

Traditional wet chemical measurements of the above-mentioned indicators are comparably slow and usually expensive, so faster techniques are sometimes needed to replace or supplement them

and especially techniques that provide robust data. The wet chemical analysis gives direct (quantitative) chemical information but with limited depth/time resolution. This is where near-infrared (NIR) spectroscopy can be helpful.

In soil-sedimentary contexts, NIR applications have been tested to analyze soil characteristics (Udelhoven, Emmerling, & Jarmer, 2003, Viscarra Rossel, Walvoort, McBratney, Janik, & Skjemstad, 2006). In examples of studies in archaeology, NIR spectroscopy has been used to further enhance remote sensing sensibility (Grøn et al., 2011). Here it was shown that hyperspectral image analysis could be used for identifying archaeological features. Matney et al. (2014) presented an archaeological prospection study where it was shown that in situ shallow subsurface features, such as hearths and storage pits could be spectrally identified. Araújo et al. (2015) used NIR spectroscopy to study Amazonian dark Earths to predict soil properties, such as soil organic carbon etc, using Partial Least Squares regression (PLS) modeling. The outcome of this study was that most parameters except soil P could be successfully predicted. Bone materials in archaeological contexts have been studied by several authors with different approaches. In Thomas et al. (2011) and Linderholm, Fernández Pierna, Vincke, Dardenne, and Baeten (2013) the use of NIR hyperspectral imaging was used to analyze bone taphonomy in different contexts. Furthermore, Cascant et al. (2017) provides a NIR study on how to predict alkaline earth elements in bone remains using PLS predictive modeling. Examples of using NIR-Imaging techniques in field was done at the fortified city of Carcassonne where walls and mortars were analyzed in situ (Allios et al., 2016).

In archaeology, sedimentation, stratigraphic development, and depth are related to time: the deeper the sample is taken the older it is. Gradients in depth of chemical concentrations give an indication of human activities over time. We aim to show that also gradients in NIR spectra have this functional relationship. For the analyses presented in this paper, soil material was collected during an archaeological excavation in 2005, from a trench covering a full depth profile (from top to subsoil). The samples were analyzed by different wet chemical and physical methods in the lab and the same samples were again analyzed in 2016 when also NIR spectroscopy/imaging was conducted using three different NIR instruments. Figure 1 explains how the different samples were presented to the analysis methods. The schematic trench profile is presented in this figure. More details are given in the methods and materials section. The spectroscopic data has the potential of giving better spatial and time resolution, however, this requires finding a relation between wet chemistry and spectral response. The main topic of the paper is then to present a number of ways of making the spectroscopic data make sense, either on its own or in combination with the wet chemical data obtained.

NIR radiation can penetrate to a depth of a few mm into a powdered solid material. Because of a combination of refraction inside particles and reflection on surfaces (combined into transflection), some of the radiation comes out of the material again and can be measured by a sensor or collected with fiber optics. In this process also absorption occurs which gives the collected spectrum a chemical fingerprint of the material. Near Infrared spectroscopy has been used for classifying and quantifying solid materials, including soils. In this study, two different acquisition techniques have been used namely probe and imaging.

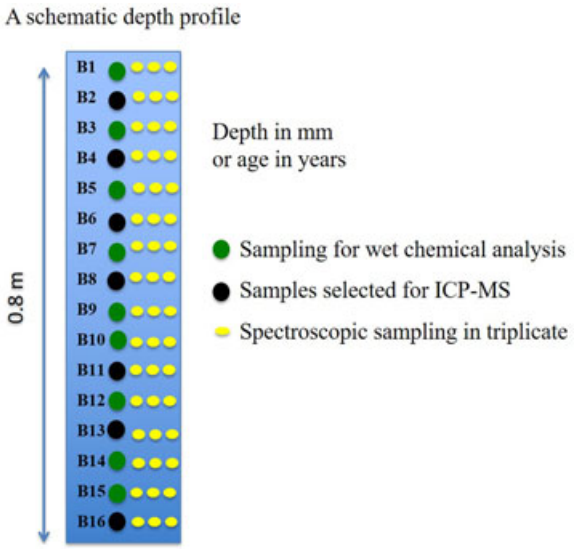

FIGURE 1 A schematic and actual view over a profile, samples (B1-B16) and measurements used in this paper. Not all wet chemical measurements could be made for all the sampled depths. Spectroscopic measurements were easy and cheap to make in triplicate using three different NIR instrumentations. NIR: near infrared [Color figure can be viewed at wileyonlinelibrary.com]

Near Infrared spectroscopic measurements have two advantages: they are faster than collecting samples in containers and analyzing them in the lab and, therefore, they can provide a higher resolution in time (more depths) and they are nondestructive. Furthermore, spectra can be collected in field/in situ. A field instrument probe can just be pointed towards a spot in the excavation. Besides NIR spectroscopy in the field, in-field hyperspectral imaging would also be a possibility, allowing a direct spatialization of the spectral information. We were unable to carry out imaging in field, but include a comparison based on laboratory imaging. Another important issue is that in an ideal situation, the scarce sample based wet chemical and abundant in situ spectroscopic information can be related by a regression model so that the wet chemical parameters can be predicted also with higher spatial and temporal resolution.

2 | MATERIALS AND METHODS

2.1 | The bastuloken site

The soil sequence that has been analyzed derives from the Neolithic site Bastuloken, Raä 158, Ramsele parish, Ångermanland Sweden (N 63° 40.3622′/E 16° 24.1107′) (Figure 2). The site is located on a sandy glacifluvium with dominating vegetation of pine (*Pinus sylvestris*), assorted lichens (*Cladonia*), blueberry and lingonberry (*Vaccinium*). Acid Podzols is the general soil type with well-developed eluviation- and illuviation horizons and subsequent translocation of

FIGURE 2 Overview of Sweden and the site Bastuloken (raä 183, Ramsele parish, Ångermanland, Northern Sweden) [Color figure can be viewed at wileyonlinelibrary.com]

elements such as Fe-Al through the soil profile (Melkerud, Bain, Jongmans, & Tarvainen, 2000).

At this site, four oval semisubterranean structures (embankments) have been localized and three of them in close connection to the lake Bastuloken. The site has been excavated on three occasions and several phases were observed in the sedimentation of the walls (Engelmark & Harju 2005, Larsson, 2010, Larsson, Rosqvist, Ericsson, & Heinerud, 2012). The embankments consisted of large amounts of unburned elk bones, fire-cracked stones, reaching a height of 0.8–1 m above the initial soil surface (Storå, Strand & Fridén-Rolstadaas, 2011). Artefacts were predominantly scrapers, slate points and general lithic debris (Engelmark & Harju 2005, Larsson et al., 2012, Linderholm et al., 2013). It is quite clear that massive hunting activities were going on at the site but the scale of bone amounts deposited, point toward activities dealing with more than just food production and consumption. Large scale elk skin processing is one suggested activity connected to these constructions.

Relating depth with time ^{14}C dating is useful and these data are available Larsson (2010) and Larsson et al. (2012). The ^{14}C analysis from these studies showed initial dates to the late Neolithic (approximately 2500 BC) and encompasses 600-year span from base to top of the profile sequences.

2.2 | Sampling during excavation

The 2005 excavation was conducted by opening a square pit of one by one meter and excavating in 10 cm levels (Figure 3a) (Engelmark & Harju 2005). During the course of excavation every ten cm layer was sieved to 2 mm and bulk samples were collected for the analysis of macrofossils and bone while fire-cracked stones were recorded at different excavated levels of depth (DN1-DN8) (Table 1). Once the full profile was exposed, 16 depth profile samples were collected (B1-B16), every five cm from 0–80 cm depth (Figure 3b). They were dried and packaged for analysis. Before any analysis, samples were passed through a 2 mm sieve and homogenized using mechanized mortar ().

2.3 | Wet chemical and other analysis

An overview of all analyses carried out for the 16 depths is presented in Table 2. All 16 samples were analyzed using loss on ignition (LOI) at 550°C, 2% citrate soluble phosphate (Cit-P) and magnetic susceptibility (MS) (Linderholm, 2010). inductively-coupled plasma mass spectrometry (ICP-MS) measurement was only conducted on half of the samples because of time and cost considerations.

The analytical methods used to analyze the collected samples are described in some previous studies (Arrhenius, 1934, Grabowski & Linderholm, 2013, Linderholm, 2010).

In this study, the focus is on the analysis of 2% citric acid soluble, mainly inorganic phosphate (inorganic-PO4, Soil P). Human-driven accumulation and circulation of phosphate in settlement and other contexts are well known in archaeology. Loss on Ignition was performed on samples dried to constant weight (105°C) and subsequent combusting of sediment material in crucibles at 550°C for 4 hr (Carter, 1993). Usually, the LOI is assumed to correspond to the crude organic mass of the soil, but will also include partly combusted materials something that may be most significant in soil and sediments affected by human activities. MS of the soil samples was analyzed with a Bartington system (MS2 with MS2B dual sensor [Dearing, 1994]). MS is useful to characterize soils and sediments and especially in relation to processes of heating. All MS data reported here are low-frequency measurements (χlf 10^{-8} m^3kg^{-1} mass-specific susceptibility) on 10^{-g} soil samples.

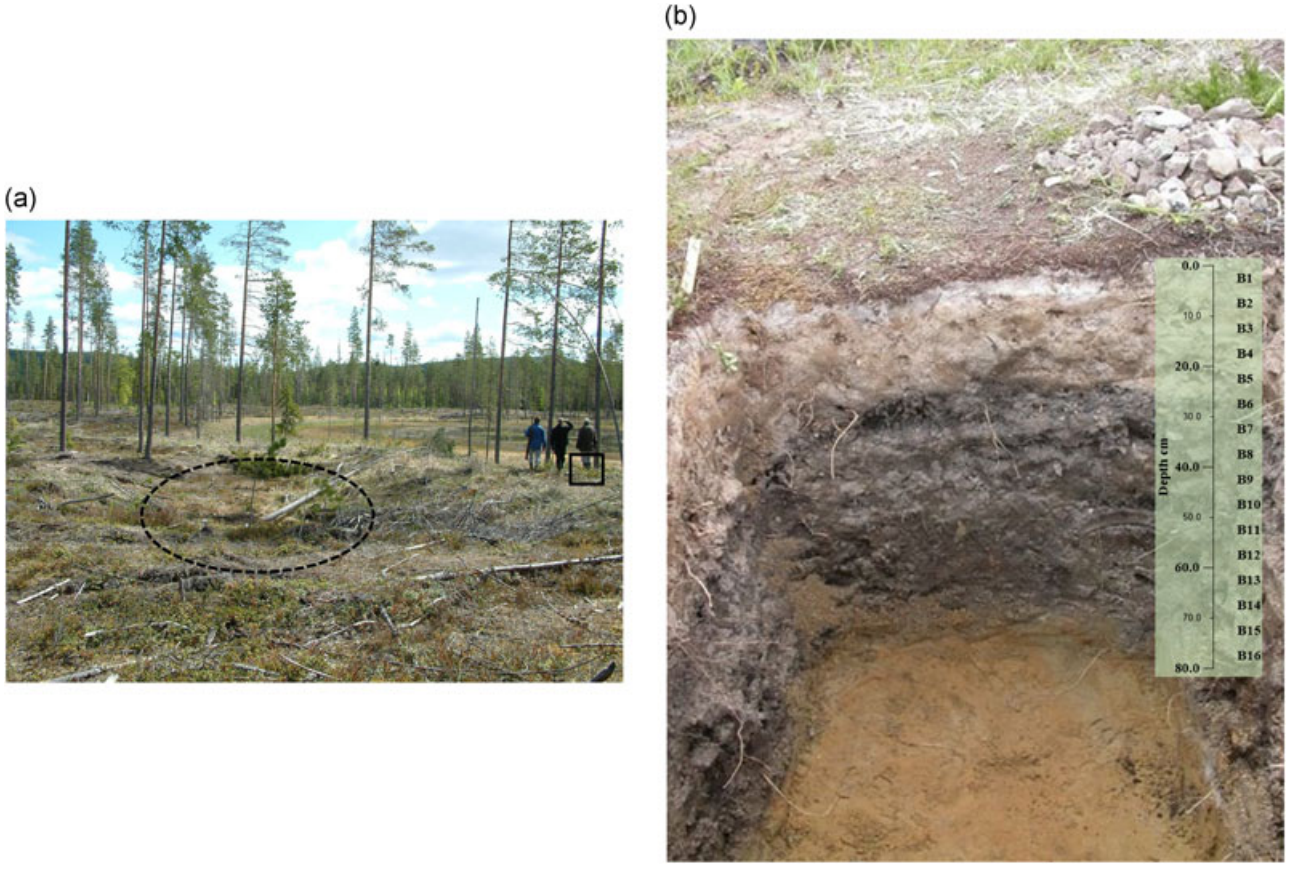

FIGURE 3 (a) Photo of one of the semisubterranean structures at Bastuloken, with the lake in the background. Inner lowest part indicated by a dotted line and the three persons are standing on the top of one embankment. A square marks the location of the excavated trench. (b) Photo of analyzed profile sequence at Bastuloken with sampled part indicated by a rectangle and sample positions marked. Note parts of the excavated fire-cracked stones in the upper right corner [Color figure can be viewed at wileyonlinelibrary.com]

A subset from 16 samples originals was selected for further analysis of ICP-MS (table 2). For the ICP-MS analysis, samples were dissolved using a mix of nitric and perchloric acids (HNO_3+$HClO_4$), in an Open beaker system. The instrumentation used was a ICP/MS-DRC-Elan 6100, Perkin-Elmer, Norwalk, Connecticut (Linderholm, 2010). Here we report data from sulfur (S), phosphorous (P) and calcium (Ca) as these elements partly represent bone matter in the analyzed context.

TABLE 1 Samples and excavation findings

Level	from	to	Fire-cracked stones (l)	Bone unburned, g
DN1	0	10	10	0
DN2	10	20	21	64
DN3	20	30	22	606
DN4	30	40	17	1,523
DN5	40	50	18	1,234.3
DN6	50	60	27	1,019.5
DN7	60	70	20	2,200.6
DN8	70	80	1	137.8

TABLE 2 Overview of analysis performed

Depth, cm	MS	LOI, %	Cit-P	S	Ca	P	NIR 3 instruments
5	+	+	+				x
10	+	+	+	*	*	*	x
15	+	+	+				x
20	+	+	+	*	*	*	x
25	+	+	+				x
30	+	+	+	*	*	*	x
35	+	+	+				x
40	+	+	+	*	*	*	x
45	+	+	+				x
50	+	+	+				x
55	+	+	+	*	*	*	x
60	+	+	+				x
65	+	+	+	*	*	*	x
70	+	+	+				x
75	+	+	+				x
80	+	+	+	*	*	*	x

Abbreviations: Cit-P: citrate soluble phosphate; LOI: loss on ignition; MS: magnetic susceptibility; NIR: near infrared.

TABLE 3 Overview of NIR instrumentation used

Instrument	Sensor	Detector	Illumination source	Wavelength range, nm	Area measured
MicroNIR	InGaAs, photodiode array 128 pixel	Probe	Two quartz halogen lamps	908–1,676	Approximately1 cm^2
ASD	InGaAs, photodiode, TE cooled	Probe, Fiber optic	Quartz halogen lamp and optical fiber	350–2,500	a few mm^2
Hyspex	HgCdTe, 320 pixels* 256 bands	Line scanning camera, with objective	Halogen lamps	961–2,489	1–16 cm^2

Abbreviations: ASD: analytical spectral devices; NIR: near infrared.

2.4 | NIR Instrumentation and spectral acquisition

In this study, three different NIR instrumentations were used. The first two techniques use either a fiberoptic probe for simultaneous illumination and collection of transflected radiation or a probe with separated illumination and collection devices in the probe head. As an imaging option a more recent technique was used, where a whole scene is illuminated and the transfected radiation is collected pixelwise in a line scanning camera, giving a complete image.

The three NIR instrumentations used were: (a) JDSU MicroNIR, (b) Analytical Spectral Devices (ASD) LabSpec 4, and (c) Hyspex line scanning camera. Technical details for the NIR instruments are presented in Table 3.

All materials analyzed by NIR were also subjected to wet chemical analysis (see Section 2.3).

2.4.1 | JDSU MicroNIR field spectrometer measurement

The JDSU MicroNIR 1700 is a portable instrument to be connected to a tablet (Windows 7 based software) or laptop computer for field work. The probe is 42 mm (diam) by 42 mm (length) in size (see also Linderholm, Geladi, & Sciuto, 2015). It is based on an InGaAs detector and two built in quartz halogen lamps and it gives absorbances for 125 wavelengths (908–1,676 nm). This is approximately a wavelength every 6 nm.

The obtained data set was thus 16 × 125. Calibration was done by using dark current for 0% and reflections from a Spectralon (Labsphere, Inc., North Sutton, NH) standard for 100%. The spectra in reflectance were transformed into absorbance. Three measurements per sample were collected and subsequently averaged. The JDSU is the only portable instrument used for the data in this paper and it is therefore important because it has a high potential for field use. Data on the MicroNIR can also be found in the references (Zumba & Rodgers, 2016, Wang et al 2015).

2.4.2 | ASD LabSpec 4 measurement

In the experimental setup for the ASD LabSpec (Analytical Spectral Devices Inc., Boulder, CO), a halogen light source (150 W) was coupled with a 940 μm core diameter optical fiber and collimated by an aspheric lens. The incident beam was a 2 cm diameter circular spot. The reflected light was collected by an optical fiber bundle (44 fibers with a 200 μm core diameter each). This fiber bundle was connected to a LabSpec 4 Bench spectroradiometer, featuring a detection range of 350–2500 nm, whose spectral sampling (resp. spectral resolution) was 1.4 nm (resp. 3 nm) in the visible and near infrared range and 1.1 nm (resp. 10 nm) in the short-wave infrared range. A constant angle of 30° was maintained between the excitation and collection arms. This angle was chosen to optimize the intensity of the reflected beam and to avoid specular reflection. For each sample, dark current was recorded from all measured spectra and subtracted. A Spectralon (Labsphere, Inc.) white reference was used as a reference to standardize spectra from nonuniformities of all components of the instrumentation. Three measurements per sample were collected and subsequently averaged to give a 16 × 2151 data matrix of absorbance values (Araújo et al., 2015, Cambou et al., 2016).

2.4.3 | Hyspex SWIR measurements

The NEO Hyspex (Norsk Elektro Optikk, Lørenskog, Norway), a push-broom hyperspectral camera was set up on a translation stage operated by a stepper motor and a computer supported by NEO software (Norsk Elektro Optikk). An illumination unit including 150 W tungsten halogen source mounted at a 45° angle was used to illuminate the sample. The hyperspectral camera covers the spectral range from 1,000–2,500 nm in 256 bands (spectral resolution of 6 nm) with 320 pixels over the cross-track field of view (FOV). The camera was equipped with a 30 cm lens that produced a nominal pixel size of approximately 0.287 mm across and 0.427 mm along the FOV, respectively (Mishra et al., 2016). Settings of acquisition parameters were performed by means of the software provided by NEO. Raw images were first corrected in radiance using sensor characteristics (e.g., spectral sensitivity) provided by the manufacturer. As acquired radiance images depended on lighting condition, a reflectance correction was performed by using a 99% reflectance Spectralon (Labsphere, Inc.) surface placed within each scene. The average reflectance spectrum from the total surface of each sample was extracted. Finally, absorbance images ($-\log_{10}$) were computed for use in further analysis.

The powdered samples were transferred from plastic bags into Al cups of 4 cm diameter for imaging. The images were cleaned of background and other irregularities and used both as images and as an average spectrum. The average spectra formed a matrix of size 16 × 256.

The Hyspex images were made into a mosaic containing all samples B1-B16 in depth order. The images contained shadows from the illumination and also reflections from the Al cups. Fortunately, a

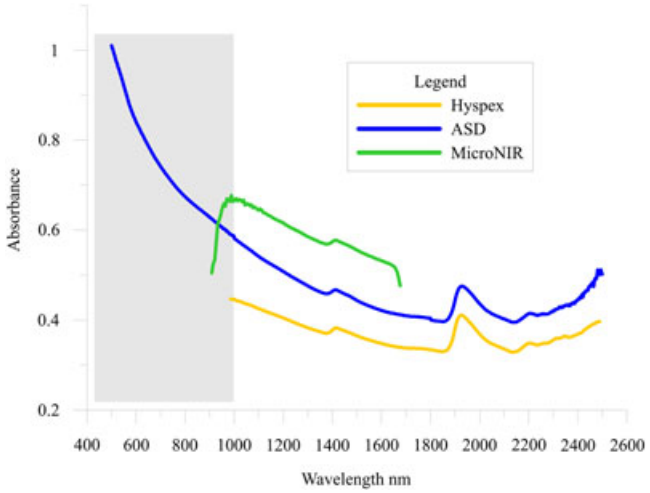

FIGURE 4 Average (Vis and) NIR spectra for three instruments MicroNIR, ASD-LabSpec 4, Hyspex (sample in aluminum cup). Spectral data in below 1,000 nm was excluded from all models. ASD: analytical spectral devices; NIR: near infrared [Color figure can be viewed at wileyonlinelibrary.com]

spot of about 1 cm^2 in the middle of each image was correctly illuminated. After some background and shading removal, an error-free square cm was extracted.

2.4.4 | Comparison of NIR spectra from the different instruments

This study focuses on the NIR wavelength range for sake of comparison and only the InGaAs detector for the ASD instrument was used for the comparison, above 1,000 nm.

Figure 4 shows an example of three different averaged spectra on the 16 samples, acquired with the three instruments. In spite of the differences in spectral range, some similar traits can be studied if a multivariate analysis is used. The visible peaks at 1,400 and 1,950 nm are related to OH bonds (water in different forms).

2.5 | Multivariate data analysis

The data produced by the NIR spectrometer and imaging equipment consisted of many variables and required multivariate data analysis. Before all analysis, all wavelengths below 1,000 nm were removed because these only represent the visible light reflection (color) of the samples.

Principal component analysis (PCA) was done to get an overview of large multivariate data sets with possibly correlated variables. A few principal components were extracted to represent the spectral information contained in the data (Wold, Esbensen, & Geladi, 1987). The Evince software was used for making and testing PCA models (Prediktera 2.7.4).

PCA was used on average spectra from the NIR probes, but also on the hyperspectral images from the NEO images. Especially in imaging, a correction for scattering and offset of each pixel spectrum is often useful. Standard normal variate correction (SNV) (Barnes, Dhanoa, & Lister, 1989) means that for each spectrum the mean is subtracted and the spectrum is divided by its standard deviation. This is an accepted method for removing specular reflection and penetration depth differences (topography) between the samples. For the hyperspectral images, SNV correction and columnwise mean-centering were used.

3 | RESULTS

3.1 | Profiles from wet chemistry

To begin with, we present the vertical profile of Cit-P, LOI, and the MS (Figure 5). First, the sequence shows a large variation in Cit-P

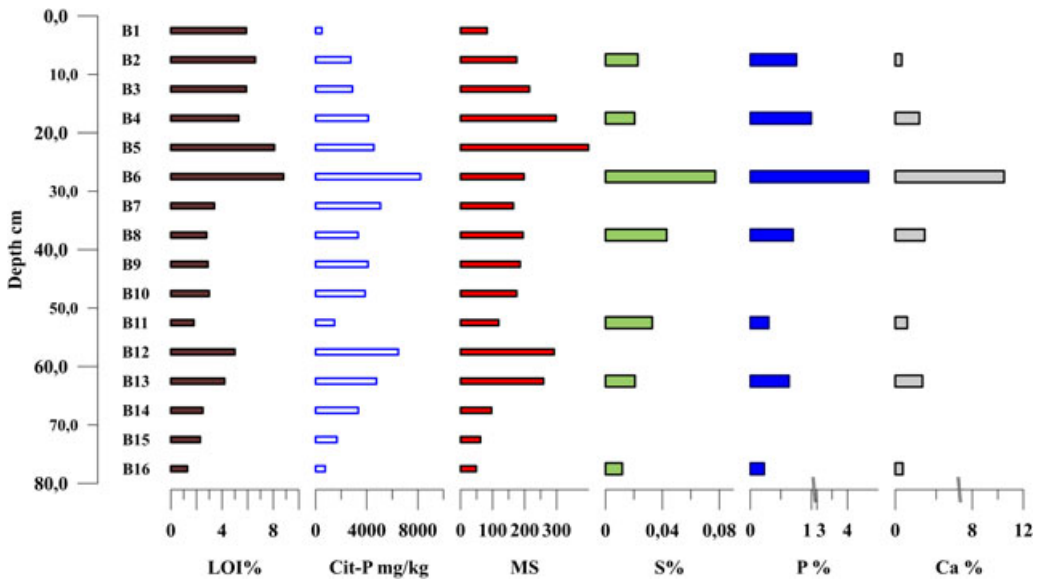

FIGURE 5 A stratigraphic compilation of samples and analytical results; loss on ignition, citric soluble phosphate and magnetic susceptibility, and ICP-MS wet chemistry data, (sulfur (S), phosphorous (P) and calcium (Ca)). ICP-MS: inductively-coupled plasma mass spectrometry [Color figure can be viewed at wileyonlinelibrary.com]

concentrations and also what appears to be two main and strong accumulation events, in this respect. This is corroborated by the MS readings that demonstrate a similar pattern. The LOI data are quite high compared to the surrounding forest podzol soils and the LOI readings show a corresponding two-peak pattern in the stratigraphic sequence. Furthermore, the data subset from the ICP-MS study for S, P, and Ca is also presented in Figure 5. These data display similar trends as the above mentioned, although the ICP-MS analyzed P concentrations are significantly higher than that of the Cit-P. Also, it should be noted the extreme levels of Ca (and P) in sample B6 (at percentage levels). These classical human indicator elements show that human activity has varied considerably over time.

3.2 | Multivariate analysis of NIR spectra

The PCA was performed on the ASD and MicroNIR spectra. Components 1 and 2 are shown for the ASD data (Figure 6). In Figure 6, the first component (t1) separates the samples in two clusters (positive-negative). On the negative side, there is also a separation in two clusters in the t2-component (positive-negative). Similar PCA clustering was also obtained with the Hyspex (not shown here). For the MicroNIR, separation of objects was found only for Component 1. The second and higher components were too noisy to show anything useful.

In Figure 6, two objects (B10-B11) do not belong to the neighboring group. This is purely based on visual observation in the figure. The clusters defined here have too few members for allowing a deeper statistical clustering analysis. However, samples closely related in depth do form clusters which make sense stratigraphically.

It is possible to see a grouping in depth and this grouping is indicated by using different colors and symbols. Class I and II (B1 and B14–16) relates to podzol soil formation as the buried (Eb-horizon) and the upper "contemporary" (E-horizon) eluviation horizon show the same characteristics. Buried B-horizon samples retain similar traits as the later formed ones. Also, the sedimentary process, where subsoil (C-horizon) material is redeposited on the top part of the profile probably also carry traits from this soil horizon. It becomes quite clear that the NIR information together with the PCA gives a good platform for identifying podzolized paleosols.

Samples B7–13 together with sample B5 form a dense group covering the mid part of the sequence. The samples B10 and B11 seem to be outliers and they both show comparably low readings in phosphate and MS. Samples B2–4 and B6 show a less dense grouping. One may assume that the non-background samples show human impact but in a different form for Class I and for Classes III and IV. This shows how PCA can be used for finding outliers (if any exist) and for classification of samples.

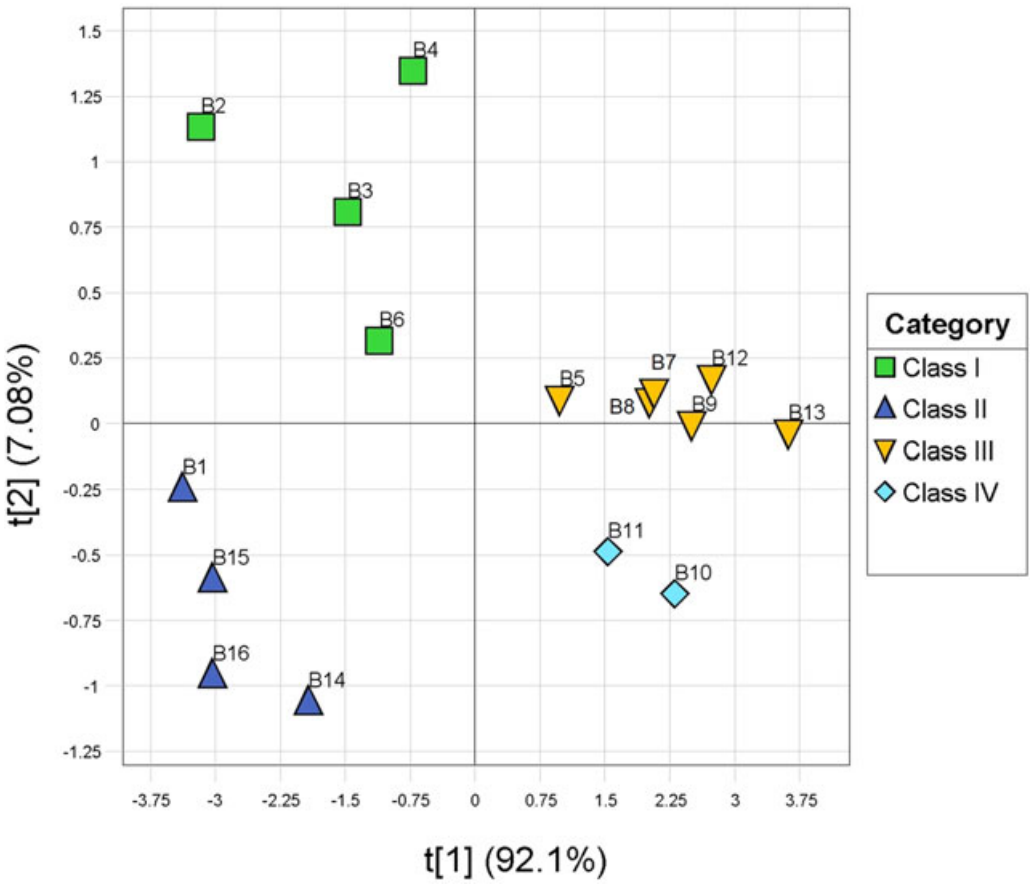

FIGURE 6 Score plot of scores t1 and t2, ASD (1,000–2,500 nm range). ASD: analytical spectral devices [Color figure can be viewed at wileyonlinelibrary.com]

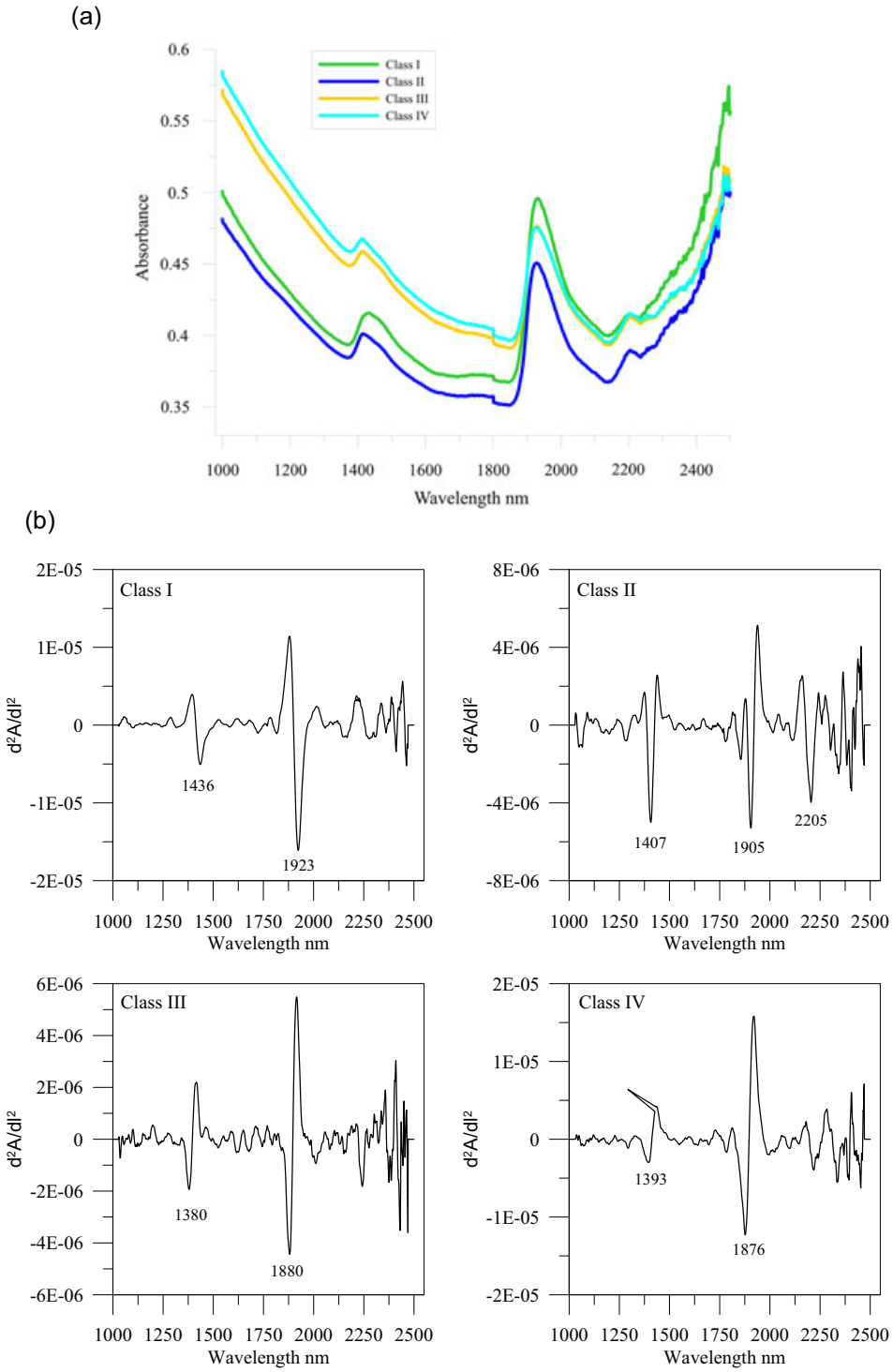

FIGURE 7 (a) Average NIR-spectra for the classes in Figure 6 (ASD). (b) Savitzky-Golay 2nd derivative on average spectra of the four classes (I-IV), with some highlighted peaks, (d^2A/dl^2; l: wavelength, A: absorbance). ASD: analytical spectral devices; NIR: near infrared [Color figure can be viewed at wileyonlinelibrary.com]

Some form of explanation of the groupings in Figure 6 can be found on average spectra as shown in Figure 7a (average spectra from each class as shown in Figure 6). Absorbances are higher when samples are dark as in the classes I and III. Differences in quality and quantity of humic matter content are the probable cause for this.

In Figure 7b, 2nd derivative spectra are shown for the four classes. The large negative peaks are identified by wavelengths of importance. Looking in detail, we see that class III and IV are characterized by minerogenic water (OH groups) at around 1385 nm and 1880 nm. On the other hand, classes I and II show very little signs of this spectral response but there are clear water-OH

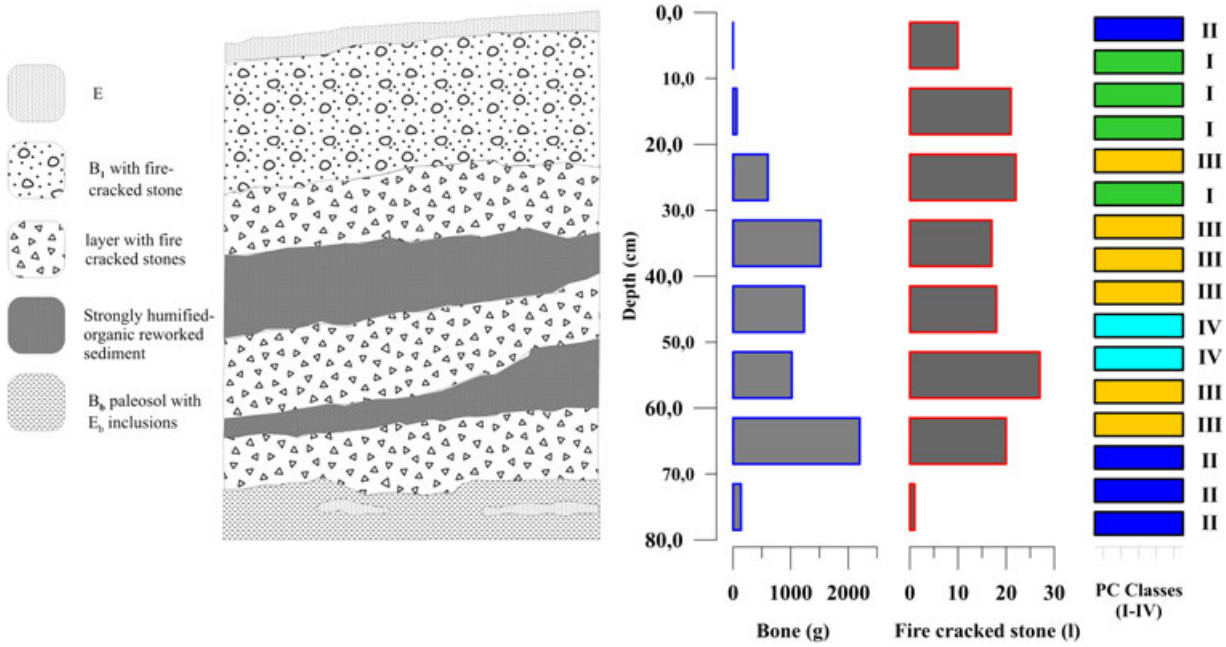

FIGURE 8 The archaeological profile interpretation and amounts of unburnt bone and fire-cracked stone in each 10 cm documentation level of one square meter. Classes added from NIR-PCA in Figure 6 (PC 1 and 2) [Color figure can be viewed at wileyonlinelibrary.com]

peaks responding 1407 nm, 1436 nm and 1905 nm, 1923 nm. In class II, a typical amino-peptide response at 2205 nm should be noted, possibly related to humic matter (Workman & Weyer, 2012).

Figure 8 combines the archaeological observations of bone material and fire-cracked stone retrieved during the cause of excavation. Also, the classes (I-IV are shown) from Figure 6 are shown in corresponding colors. There is not a perfect correspondence between NIR classes and archaeological and geological observations. However, there is an apparent sampling issue that affects this outcome. The bone/ stone observations represent a volume of 100 dm^3 that was retrieved during the cause of excavation. The subsamples used for NIR and other analysis are represented by a volume of 0,125 dm^3 and the fraction <1,25 mm. This means that the correlation between the different sample groups is not necessarily absolute. Also, the smaller samples were collected along a horizontal line in the corner of the excavated square and in that sense do not represent the full volume of the excavated volume, however, the vertical resolution is higher.

Where low amounts of bone and fire-cracked stone are recorded, this corresponds well to the soil formation processes observed in the field and also found in the NIR classification. The NIR data provides more possibilities on how to interpret the profile sequence.

Another striking observation is related to bone corrosion and erosion is evident in the upper part of the sequence, leaving high amounts of phosphate and low amounts of retrieved bones. Also, the retrieved bones from the excavation showed a reversed corrosion pattern as the oldest (deepest deposited) were the best preserved (Linderholm et al., 2013).

3.3 | Hyperspectral image analysis of the Hyspex images

The Hyspex imaging device is able to produce hundreds of thousands of pixels per image, where each pixel is a spectrum. This provides a different way of analyzing the data using imaging techniques. Two

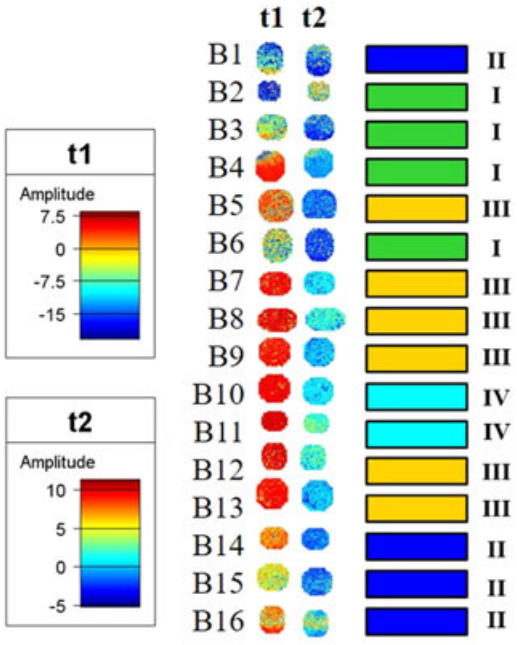

FIGURE 9 Hyspex hyperspectral results for the cleaned image. Shown are PCA t1 (left) and t2 (right) for the 16 samples (B1 top-B16 bottom) in sample cups. The variation in color represents score value. Classes from figure 8 are added for comparison [Color figure can be viewed at wileyonlinelibrary.com]

PC-components were considered meaningful to show (score t1 71,3%, score t2 7,8%) as mosaic images and in Figure 9, these 2 components are shown as depth profiles. The color of the samples indicates the score value. There is a clear distinction between the spots that conforms very well to classes found in the score plot of the ASD scores in Figure 6.

Both scores clearly show a progression in color when moving from sample level 1–16. Figure 9 shows clearly that there is a potential for also using imaging in field situations. Another advantage of imaging that is easily be seen in Figure 9 is that also inhomogeneity inside the samples can be observed and studied. Still, calculating average spectra for each image gives almost the same information as in Figure 6.

4 | DISCUSSION

The real world situation of archaeological observations is different from that of process industry or food quality assurance in that all samples are unique and final and that repeats are not possible to acquire. We only have data from the endpoint state of all previous events as in this case to understand the process forming the archaeological record. The conditions are not fully controllable or repeatable, which is a very different situation to most experimental situations. Still, the results in this study show that it is possible to use a data analysis approach similar to the process industrial one to get new information from archaeological contexts.

It was shown the NIR spectral information combined with multivariate analysis could be used to find soil horizon traits. The NIR measurements on the soils samples show that classes similar to those obtained by wet chemistry can be obtained that clearly shows the potential of using NIR spectroscopy in archaeological contexts.

The three instruments showed approximately the same potential for interpretation but the one with the largest wavelength range/spectral resolution was slightly better. The NIR-imaging data can be used for making average spectra, but it could also give images where homogeneity within a sample can be studied.

Field sampling and subsequent analysis of collected materials is still the most common way of analyzing materials from excavations. However, the spectroscopic instruments can also be taken out in the field for in situ measurements. Hyperspectral imaging for field use is still in its early stages and, usually, laboratory measurements are necessary to ensure spectral reproducibility. Imaging techniques open a way for future studies where intact profiles are documented with spectroscopic and spatial information and less physical sampling is needed.

Images have the advantage of allowing two modes of measurement. It is possible to integrate an area in the image to obtain an integrated spectrum that is comparable to that of the spectrometers. It is also possible to study the images for spatial information on particle size and distribution. For some types of materials, this image mode is necessary. If NIR measurement and Imaging can be developed for use in the field then potentially less soil sampling is needed. The better suggestion is to use field imaging where hundreds of thousands of spectra over a large area can be collected and analyzed by hyperspectral image analysis as Figure 9 clearly shows. This would also add to the general documentation of excavations in general, combining the strength of images and chemical information.

NIR analysis provides information that enables interpretations in terms of soil formation and cultural impact intensity. Improved understanding of this process and the nature of these soils will improve the understanding of the cultural processes forming them. This is where NIR spectroscopy is helpful. The paper describes a test of this idea on one stratigraphy but the results can be generalized to a more complete analysis.

ACKNOWLEDGMENTS

Marcus & Amalia Wallenberg Foundation (MAW 2012.0136) and The Kempe Foundation (SMK-1749) for financial support. The authors would also like to thank the three anonymous reviewers for constructive comments.

ORCID

Johan Linderholm http://orcid.org/0000-0001-7471-8195

REFERENCES

Allios, D., Guermeur, N., Cocoual, A., Linderholm, J., Sciuto, C., Geladi, P., … Gardel, M. E. (2016). Near infrared spectra and hyperspectral imaging of medieval fortress walls in Carcassonne: A comprehensive interdisciplinary field study. *NIR news*, *27*, 16–20. https://doi.org/10.1255/nirn.1602

Araújo, S. R., Söderström, M., Eriksson, J., Isendahl, C., Stenborg, P., & Demattê, J. A. M. (2015). "Determining soil properties in Amazonian Dark Earths by reflectance spectroscopy.". *Geoderma*, *237–238*(0), 308–317.

Arrhenius, Olof (1934). Fosfathalten i skånska jordar. Sveriges Geologiska Undersökningar. Ser C, no 383. *Årsbok*, *28*(3), 1–32.

Barnes, R. J., Dhanoa, M. S., & Lister, S. J. (1989). Standard Normal Variate Transformation and De-trending of Near-Infrared Diffuse Reflectance Spectra. *Applied Spectroscopy*, *43*, 772–777.

Cambou, A., Cardinael, R., Kouakoua, E., Villeneuve, M., Durand, C., & Barthès, B. G. (2016). Prediction of soil organic carbon stock using visible and near infrared reflectance spectroscopy (VNIRS) in the field. *Geoderma*, *261*, 151–159.

Carter, M. R. (1993). *Soil sampling and methods of analysis*. London: Lewis Publishers.

Cascant, M. M., Rubio, S., Gallello, G., Pastor, A., Garrigues, S., & de la Guardia, M. (2017). Prediction of alkaline earth elements in bone remains by near infrared Spectroscopy. *Talanta*, *162*, 428–434.

Dearing, J. (1994). Environmental magnetic susceptibility: Using the Bartington system, *Bartington Instruments*. London.

Engelmark, R. & Harju, J. (2005). Rapport över arkeologisk förundersökning av Raä 183, Ramsele sn, Ångermanland, 2005. Umeå: Institutionen för arkeologi och samiska studier, Umeå universitet.

Goldberg, Paul, & Macphail, Richard I. (2006). *Practical and theoretical Geoarchaeology*. Malden, Mass: Blackwell.

Grabowski, R., & Linderholm, J. (2013). Functional interpretation of Iron Age longhouses at Gedved Vest, East Jutland, Denmark: Multiproxy analysis of house functionality as a way of evaluating carbonised botanical assemblages. *Archaeological and Anthropological Science*, *6*(4), 329–343.

Grøn, O., et al. (2011). "Interpretation of archaeological small-scale features in spectral images.". *Journal of Archaeological Science*, *38*(9), 2024–2030.

Holliday, V. T., & Gartner, W. G. (2007). Methods of soil P analysis in archaeology. *Journal of Archaeological Science*, *34*, 301–333.

Larsson, T. B. (2010). Människan och älgen vid Bastuloken: En delundersökt boplatsvall från neolitikum i Västernorrland. Arkeologi i Norr. 12, 1-16. Umeå universitet.

Larsson, T. B., Rosqvist, G., Ericsson, G., & Heinerud, J. (2012). Climate Change, Moose and Humans in Northern Sweden 4000 cal. yr BP. *Journal of Northern Studies*, *6*(1), 9–30.

Linderholm, J., (2010). The Soil as a Source Material in Archaeology: Theoretical Considerations and Pragmatic Applications. Archaeology and Environment 25. Umeå Universitet.

Linderholm, J., Geladi, P., & Sciuto, C. (2015). Field-based near infrared spectroscopy for analysis of Scandinavian Stone Age rock paintings. *Journal of Near Infrared Spectroscopy*, *23*, 227–236.

Linderholm, J., Fernández Pierna, J. A., Vincke, D., Dardenne, P., & Baeten, V. (2013). Identification of fragmented bones and their state of preservation using near infrared hyperspectral image analysis. *Journal of Near Infrared Spectroscopy*, *21*, 459–466.

Matney, T., Barrett, L. R., Dawadi, M. B., Maki, D., Maxton, C., Perry, D. S., … Whitman, L. G. (2014). In situ shallow subsurface reflectance spectroscopy of archaeological soils and features: A case-study of two Native American settlement sites in Kansas. *Journal of Archaeological Science*, *43*, 315–324.

Melkerud, P. -A., Bain, D. C., Jongmans, A. G., & Tarvainen, T. (2000). Chemical, mineralogical and morphological characterization of three podzols developed on glacial deposits in Northern Europe. *Geoderma*, *94*, 125–148.

Mishra, P., Cordella, C. B., Rutledge, D. N., Barreiro, P., Roger, J. M., & Diezma, B. (2016). Application of independent components analysis with the JADE algorithm and NIR hyperspectral imaging for revealing food adulteration. *Journal of Food Engineering*, *168*, 7–15.

Storå, J., Strand, L. & Fridén-Rolstadaas, M. (2011). Osteologisk analys av obrända och brända skelettfynd från stenålderslokalen Bastuloken Raä 183, Ramsele sn, Västernorrlands län ['Osteological analysis of unburnt and bunt skeleton findings from the Stone Age site Bastuloken, Raä 183, Ramsele parish, County of Västernorrland'] (Rapport 2011:10), Osteologiska forskningslaboratoriet, Stockholm: Stockholm University.

Thomas, D., et al. (2011). "Near infrared analysis of fossil bone from the Western Cape of South Africa.". *Journal of Near Infrared Spectroscopy*, *19*(3), 151–159.

Udelhoven, T., Emmerling, C., & Jarmer, T. (2003). Quantitative analysis of soil chemical properties with diffuse reflectance spectrometry and partial least-square regression: A feasibility study. *Plant and Soil*, *251*(2), 319–329.

Viscarra Rossel, R. A., Walvoort, D. J. J., McBratney, A. B., Janik, L. J., & Skjemstad, J. O. (2006). Visible, near infrared, mid infrared or combined diffuse reflectance spectroscopy for simultaneous assessment of various soil properties. *Geoderma*, *131*(1), 59–75.

Wang, N. N., Shen, B. H., Zhao, Z. R., Zhu, Y. W., Zhang, L. D., Yan, Y. L., … Kang, D. M. (2015). Detection of adulteration in milk powder with starch near infrared. *Spectroscopy and Spectral Analysis*, *35*(8), 2141–2146. https://doi.org/10.3964/j.issn.1000-0593(2015)08-2141-06

Wold, S., Esbensen, K., & Geladi, P. (1987). Principal component analysis. *Chemometrics and Intelligent Laboratory Systems*, *2*(1987), 37–52.

Workman, J., & Weyer, L. (2012). *Practical guide and spectral atlas for interpretive near-infrared spectroscopy*. Boca Raton: CRC Press.

Zumba, J., & Rodgers, J. (2016). Cotton micronaire measurements using small portable near-infrared (NIR) analyzers. *Applied Spectroscopy*, *70*(5), 794–803. Special Issue: SI. http://prediktera.se/

How to cite this article: Linderholm J, Geladi P, Gorretta N, Bendoula R, Gobrecht A. Near infrared and hyperspectral studies of archaeological stratigraphy and statistical considerations. *Geoarchaeology*. 2019;34:311–321. https://doi.org/10.1002/gea.21731